Medical Engineering & Physics 31 (2009) 1095–1103

Contents lists available at ScienceDirect

Medical Engineering & Physics

journal homepage: www.elsevier.com/locate/medengphy

Electric field distribution in a finite-volume head model of deep brain stimulation

Peadar F. Grant*, Madeleine M. Lowery

University College Dublin, School of Electrical, Electronic and Mechanical Engineering, Dublin 4, Ireland

ARTICLE INFO

Article history:
Received 22 December 2008
Received in revised form 6 July 2009
Accepted 7 July 2009

Keywords:
Deep brain stimulation
Finite element model
Volume conduction

ABSTRACT

This study presents a whole-head finite element model of deep brain stimulation to examine the effect of electrical grounding, the finite conducting volume of the head, and scalp, skull and cerebrospinal fluid layers. The impedance between the stimulating and reference electrodes in the whole-head model was found to lie within clinically reported values when the reference electrode was incorporated on a localized surface in the model. Incorporation of the finite volume of the head and inclusion of surrounding outer tissue layers reduced the magnitude of the electric field and activating function by approximately 20% in the region surrounding the electrode. Localized distortions of the electric field were also observed when the electrode was placed close to the skull. Under bipolar conditions the effect of the finite conducting volume was shown to be negligible. The results indicate that, for monopolar stimulation, incorporation of the finite volume and outer tissue layers can alter the magnitude of the electric field and activating function when the electrode is deep within the brain, and may further affect the shape if the electrode is close to the skull.

1. Introduction

Over the last decade, deep brain stimulation (DBS) has become established as an effective therapy for symptomatic suppression of medically refractory Parkinson's disease. Although highly effective in suppressing bradykinesia, rigidity and resting tremor, its mechanisms of action remain largely unknown. It has been suggested that deep brain stimulation may cause activation or functional ablation of target neural structures, or that the stimulation may modulate neuropathological processes [1,2]. In addition, programming of the stimulator is generally performed through trial-and-error, a process which is time consuming and may not necessarily identify the optimal stimulus setting [3]. To understand the underlying mechanisms of DBS and optimize the design of stimulus protocols, an accurate estimate of the electric field distribution in the region of tissue around the DBS electrode is first required. This may then enable the effect of the stimulus on individual neurons and the dynamics of neural networks in the basal ganglia to be predicted. Quantitative analyses of alternative applications of deep brain stimulation, such as in the treatment of epilepsy, obsessive compulsive disorder, Tourette syndrome and depression similarly require accurate predictions of volume conductor effects in the vicinity of the electrode [4–7].

Volume conduction modeling provides a means of estimating the electric field distribution due to bioelectric and applied electric and magnetic sources. It is widely used in a range of applications including electroencephalography, functional electrical stimulation and more recently DBS. Current computational electromagnetic models of DBS focus on effects in the region of tissue immediately surrounding the stimulation electrode, typically within 50 mm of the electrode contact [8–10]. In such models, the tissue medium is generally represented by a simple geometric primitive such as a cube or cylinder, with the electrical ground applied over all the outer boundary surfaces [11–14]. The application of this boundary condition provides a means of approximating a situation where the electrode lies in an isotropic medium of infinite extent for which conditions at the outer extremity do not affect the solution near to the electrode. While the finite nature of the volume conductor has been shown to affect the distribution of the electric field in modeling electroencephalogram [15,16], electromyogram [17] and transcranial magnetic stimulation [18], it is not clear whether it could also have an effect on the electric field due to deep brain stimulation.

In clinical practice, the stimulation system is configured such that the reference electrode is located on the case of the implanted pulse generator which is implanted into the chest cavity. Monopolar stimulation, using one or more electrode contacts has been recommended as a preferred configuration as it requires lower stimulation currents [3,19]. Bipolar stimulation is used where a more spatially focal stimulus is desired, and is less likely to elicit side effects than monopolar stimulation as the stimulus voltage is increased [20]. Under monopolar conditions the material properties of the surrounding tissue medium and the location and extent of the electrical ground determine the strength and direction of the

* Corresponding author. Tel.: +353 876331729.
E-mail address: peadar.grant@ucd.ie (P.F. Grant).

1350-4533/$ – see front matter © 2009 IPEM. Published by Elsevier Ltd. All rights reserved.
doi:10.1016/j.medengphy.2009.07.006

electric field surrounding the electrode. Previous models of deep brain stimulation have assumed that the electrode lies in a large homogeneous, isotropic medium of infinite extent, since electrical ground will not influence the contour of the electric field. To represent this condition in such models, a zero-potential boundary condition has been applied to all outer surfaces of the volume conductor [11,12,14]. Due to lack of a more detailed formulation, this technique ensures that the geometry of the conducting volume does not have an undue influence on the solution by influencing the return current path in an asymmetric fashion. However if the location of the stimulator in the trunk and the surrounding layers of differing electrical conductivity are considered, it is likely that the electric field will vary depending on the location of the electrode in the volume conductor. In the case of bipolar stimulation, however, it is possible that the effect of the finite conducting volume and outer layers may be less significant. Since in this study we chose to use a finite-volume model in which the head's enclosed volume is explicitly included, it was necessary to choose the manner in which the reference electrode is represented.

The aim of this study was to examine the effect of electrical grounding and the finite conducting volume of the head on the electric potential, electric field and the activating function [21] in the tissue immediately surrounding a monopolar DBS electrode, using an idealized finite element head model. An idealized model enables the effect of parameter variation, such as material properties, to be examined without compounding effects due to subject-specific anatomical variations. While a large number of simplified geometries exist for applications such as electroencephalography, transcranial magnetic stimulation and radiology [15,18,22], no whole-head models have yet been presented in the literature with specific application to intracranially implanted electrical stimulation. While this study focuses on deep brain stimulation, related problems also occur in other applications of electrical stimulation in finite volumes such as cortical stimulation, cochlear implants and retinal implants [23].

2. Methods

Three-dimensional finite element models were constructed of an idealized head geometry using COMSOL Multiphysics 3.4 (COMSOL Inc., Burlington, MA). The models incorporated an electrode based on the Medtronic 3387 electrode (Medtronic Inc., Minneapolis, MA), piecewise homogeneous skull and scalp layers, cerebrospinal fluid and the electrode encapsulation tissue, which forms at the interface between a chronically implanted electrode and the surrounding tissue layers.

2.1. Geometry

An idealized ellipsoidal geometry was created to represent the intracranial conducting volume of an adult human head and outer layers of cerebrospinal fluid, scalp and skull. The semi-axes of the bulk tissue were estimated to be 70 mm, 82.5 mm and 65 mm in the x', y' and z' directions respectively [24].

The bulk tissue was encased within the skull which consisted of a 3.0 mm thick layer of cancellous bone surrounded on both sides by layers of cortical bone, 0.75 mm thick [24]. This was surrounded in turn by the scalp which consisted of a layer of 3.1 mm thick subcutaneous fat surrounded by a 2.4 mm thick layer of skin [25].

The cerebrospinal fluid compartment has been reported to occupy a volume of approximately 1×10^{-4} m^3 [24]. It was assumed that the cerebrospinal fluid was represented by a thin layer lying within the skull, yielding an estimated thickness of the cerebrospinal fluid layer of 1.782 mm.

A Medtronic 3387 electrode [26] of radius 0.635 mm and contact height 1.5 mm was included in the model. The electrode was placed at the site of the subthalamic nucleus, which was located using a brain atlas [27]. Upon implantation of DBS electrodes, the inflammatory response of the body causes an encapsulating layer consisting of collagen, fibroblasts and giant cells to develop in the tissue surrounding the electrode. The exact composition and thickness of such tissue depends on the biocompatibility of the implant, which is a function of the shape, surface morphology and constituent materials of the implant [28]. In this study the encapsulation tissue was simulated with a 0.1 mm thick layer of resistive tissue. The interior of the DBS lead and the area outside the conducting volume were specified as unmeshed free space, into which no current can flow.

The stimulator case, located in the chest cavity provides the reference electrode which determines the path taken by the return current. In this study, it was assumed that the spinal cord is comprised of isotropic brain tissue and that it continues through the site where the spinal cord intersects the skull. It was further assumed that all of the current leaving the head exits through this site. The integral of the current density over the surface of the reference electrode is thus equal to that over the surface of the stimulating electrode.

In addition to the ellipsoidal model, a cubic model with all exterior boundaries set to 0 V was constructed. The cubic model of side 50 mm, denoted Model I was comprised of isotropic brain tissue with a Medtronic 3387 electrode located at the center of the model (Fig. 1(a)). Three variants of the idealized model were then constructed (Models II–IV). A homogeneous model was examined in which the head was represented entirely as an ellipsoidal volume of brain tissue (Model II). Another model included the skull and scalp layers and neglected the cerebrospinal fluid (Model III). Model IV incorporated skull, scalp and cerebrospinal fluid layers in full (Fig. 1(b)). The anatomical geometry of Models I–IV is summarized in Table 1. The Cartesian x direction runs along the medial–lateral direction through the head, while the Cartesian y direction runs posterior to anterior and the Cartesian z direction runs vertically through the head as indicated in Fig. 1(a).

2.2. Material properties

The brain was assumed to consist of isotropic tissue of conductivity 0.27 S/m [29]. The conductivity of cerebrospinal fluid was assumed to be 1.6 S/m assuming human body temperature of 37 °C [30]. Tissue properties for the scalp and skull were assigned from data reported in Gabriel et al. at a frequency of 2560 Hz, which represents the median frequency of one typical waveform used for deep brain stimulation (pulse width 100 μs, frequency 130 Hz) [31]. The encapsulation tissue was assigned a conductivity 0.042 S/m [28]. A summary of tissue properties used in the model is presented in Table 1.

2.3. Equation system

Under static conditions the system is governed by Laplace's equation (1) where $\phi(x, y, z)$ is the electric potential at the point (x, y, z), σ is the conductivity of the region containing the point (x, y, z) and ∇ is the gradient differential operator [32]. It was assumed that the region of interest has no space charge density and that there were no internal current sources in the tissue. A DC static analysis was considered:

$$-\nabla \cdot \sigma \nabla \phi = 0 \quad (1)$$

Laplace's equation is extendible to piecewise homogeneous media using appropriate interface conditions conserving current density.

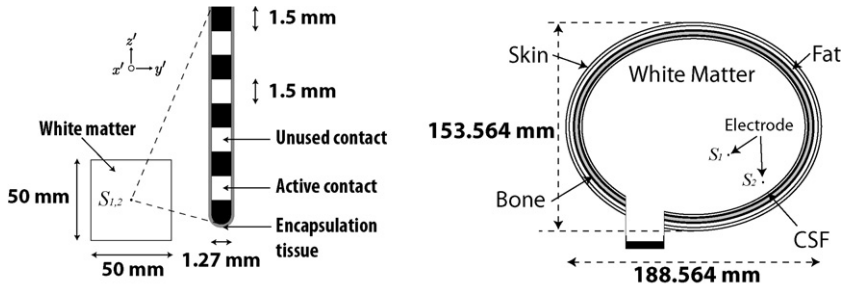

(a) Model I and DBS electrode (b) Model IV

Fig. 1. Schematic diagram of Models I and IV. The electrode geometry is shown in the inset of (a). The ground reference entirely covers the outer surface of Model I in (a) and is indicated by the black bar in Model IV (b). Two electrode positions S_1 and S_2 are shown representing the electrode's location in the region of the subthalamic nucleus and 3.5 mm from the skull boundary respectively.

Table 1
Tissue conductivities, σ, and thicknesses, d, used in model. Conductivities are calculated at a median frequency of 2560 Hz. The default values for brain and encapsulation tissue are shown.

Layer	d (mm)	σ (S/m)
Scalp		
Skin	2.4 [25]	0.00087 [31]
Fat	3.1 [25]	0.042 [31]
Skull		
Outer cortical	0.8 [24]	0.020 [31]
Cancellous	3.0 [24]	0.076 [31]
Inner cortical	0.8 [24]	0.020 [31]
Cerebrospinal fluid	1.8 [24]	1.60 [30]
Brain tissue (default)		0.27 [29]
Encapsulation tissue (default)	0.1 [13]	0.042 [28]

Dirichlet boundary conditions were enforced at the surface where the stimulus was applied and at the electrical grounding point, explicitly specifying the electric potential ϕ on these boundaries. Exterior insulating boundaries and internal boundaries were subject to current density constraints to preserve continuity.

2.3.1. Excitation

The electric potential on the surface of the most distal contact of the Medtronic 3387 electrode, ϕ_0, was set to −1 V DC.

2.3.2. Exterior boundaries

All exterior boundaries, except those on which Dirichlet conditions were enforced, were specified as insulating boundaries (2) where the normal component of the current density is zero, where $\vec{J}$ is the current density vector and $\hat{n}$ is a unit vector normal to the boundary in question.

$$\hat{n} \cdot \vec{J} = 0 \tag{2}$$

2.3.3. Interface conditions

Laplace's equation can extend to multiple piecewise homogeneous regions provided that at the boundary between any two regions, the normal component of the current density leaving one region $\vec{J}_1$, is equal to that entering the adjoining one, $\vec{J}_2$, and with $\hat{n}$ denoting a unit vector normal to the boundary surface.

$$\hat{n} \cdot (\vec{J}_2 - \vec{J}_1) = 0 \tag{3}$$

2.4. Reference

To examine the effect of the choice of reference electrode and to enable the most accurate physical approximation of the reference electrode to be chosen, two separate current return conditions were examined.

2.4.1. Localized surface return electrode

In Models II–IV the bulk tissue extends cylindrically from the brain through the cerebrospinal fluid, skull and scalp layers and is terminated within 2 cm of the scalp surface (Fig. 1). This boundary is designated as the reference electrode, using the ground boundary condition, which enforces a Dirichlet zero-potential condition on the reference surface. The reference surface is 2.8 cm in diameter, representing a surface area of 3.064×10^{-4} m^2.

2.4.2. Uniform surface return

In Model I the electrode was surrounded by a cubic block of tissue of side 50 mm. All exterior surfaces were designated as the reference electrode by applying a zero-potential boundary condition as in previous studies [11–14].

2.5. Discretization

The representative geometry was discretized in space using approximately 300,000 three-dimensional tetrahedral finite elements. Free meshes were generated using the Delaunay meshing algorithm. Smaller mesh elements were used near fine geometric details and where it was assumed that the gradient of the electric potential would be greater. Extension of the mesh used Lagrange cubic expansion functions in order that the second spatial derivative of the electric potential had linear variation across each element while reducing the number of elements required for a convergent solution.

2.6. Solution

Equation assembly resulted in approximately 1,400,000 degrees of freedom in the system matrix. The symmetric successive over-relaxation preconditioner was applied to increase the rate of convergence. The iterative conjugate gradient algorithm was used to calculate the scalar potential field and the electric field (Eq. (4)) and second spatial derivative of the electric potential in the Cartesian x and y directions.

$$E_u(u) = -\frac{\partial \phi}{\partial u} \tag{4}$$

Iterative solver convergence was enforced to 10^{-6}. It was confirmed that doubling the number of elements did not affect the electric potential by an amount greater than 1%. The solution process required 30 min on a PC workstation utilizing one Intel Core 2 Duo dual-core 64-bit processor and 4 GB of physical RAM. Solution variables were extracted along an arbitrary straight fiber axon of length 10 mm located up to 5 mm away from the central axis of the electrode at 1 mm intervals. The reference three-dimensional co-ordinate system for each electrode location has its origin at the geometric centroid of the active electrode contact. The central axis

Table 2
Impedance between the stimulating electrode and ground under monopolar conditions for each model in Table 2.

Model	Impedance (Ω)	
	Encapsulation layer included	Encapsulation layer excluded
I	750	440
II	950	640
III	1040	730
IV	1020	710

of the electrode shaft is denoted the z'-axis. The x' and y' axes lie in the anterior–posterior and medial–lateral directions respectively. The postprocessing co-ordinate system (x, y, z), which represents the direction of the fiber axons, is related to the reference co-ordinate system (x', y', z') by rotating about the z'-axis by azimuth α and about the y'-axis by elevation β. Both co-ordinate systems share the same origin. For comparative purposes, two cases of plane orientation were examined. In the first (untilted case) the xy plane was identical to the reference $x'y'$ plane since the fiber was perpendicular to the electrode. In the second case the fiber lay along a line from the origin at the center of the model to the electrode with $\alpha = 62^\circ$ and $\beta = 76^\circ$. These angles result from continuing a straight line from the geometric centroid of the concentric ellipsoids, through the tip of the electrode and onwards until it intersects the cerebrospinal fluid.

The activating function $A(u)$ as presented in Ref. [21] is a commonly used prediction of the extent of neural activation. It is defined as the second spatial derivative (5) of the electric potential ϕ along a fiber with arbitrary direction u and enables the fiber to be segmented into predicted regions of depolarization and hyperpolarization. It is assumed that the fiber will be influenced only by the component of the activating function (and electric field) that is parallel to it.

$$A_u(u) = \frac{\partial^2 \phi(u)}{\partial u^2} \tag{5}$$

To estimate the regions activated by the stimulus, a threshold can be applied to the value of $A_u(u)$ to separate the domain into regions of activation or inhibition.

2.7. Simulation details

The electric field distributions predicted by Models I–IV were compared. The sensitivity of the solution was also examined with respect to changes in the conductivity of the skull, bulk tissue and encapsulation tissue, to ascertain whether the magnitude of the effect of the layers was sensitive to changes in the tissue material properties. The conductivity of the bulk tissue and encapsulation tissue were varied between 0.05 S/m and 0.03 S/m, and 0.05 S/m and 0.02 S/m respectively [13]. The conductivities of the skull bone layers were varied between 0.5 and 2 times their original values.

Finally, the effect of the finite conducting volume and outer layers was examined for the case of bipolar stimulation at position S_1. The most distal contact was designated as the cathode, while the three remaining contacts sequentially applied the anodic stimulus.

3. Results

3.1. Impedance

The electrode impedance as estimated for the four cases under consideration are summarized in Table 2. The impedance observed between the stimulation electrode and the return electrode is purely resistive in this case and was obtained by integrating the current density over the active surface area of the electrode to obtain in the injected current. The impedance is then calculated using Ohm's law since the stimulus voltage is known.

With encapsulation tissue included, the homogeneous cubic model (Model I) had an impedance of 750 Ω. The finite volume (Model II) and finite volume with all outer tissue layers except cerebrospinal fluid (Model III) had an impedance of 950 Ω and 1040 Ω respectively, when the localized surface reference was applied to both models. The addition of the cerebrospinal fluid (Model IV) slightly reduced the impedance to 1020 Ω. Clinical impedance measurements have been reported to lie in the range of 500–1500 Ω [3,33]. Based on this range, all models lay within clinically reported values, when encapsulation tissue was included. The impedance of Model I lay outside clinically measured values when encapsulation tissue was not present.

3.2. Electrode located in STN

The electric potential, electric field and activating function resulting from an electrode located at the estimated site of the STN were compared in each of the models. Fig. 2 shows the electric potential, electric field and activating function for models I–IV plotted along two representative fiber axons. One fiber is parallel to the x-axis at a distance −3 mm from the central axis of the stimulating electrode (2.265 mm from the contact surface). The other fiber is parallel to the y-axis and is −3 mm away from the stimulating electrode.

Incorporation of the finite volume (Model II) raised the magnitude of the electric potential by approximately 150% in the example of a fiber parallel to the x-axis, 3 mm away from the central axis of the electrode. This effect was accentuated by the addition of the outer scalp and skull layers (Model III), which increased the difference in potential between the two models to approximately 278%. Inclusion of the more conductive cerebrospinal fluid (Model IV) reduced the effect of the layers slightly, reducing the difference to approximately 250% with respect to the surface grounded homogeneous model.

In the case of the electric field (Fig. 2(c)), the finite volume (Model II) reduced the magnitude of the electric field E_x by up to 11%, compared to the homogeneous, surface grounded model (Model I), while the finite volume with scalp and skull layers (Model III) was found to have an electric field up to 20% lower in magnitude than Model I. Inclusion of the cerebrospinal fluid in Model IV slightly reduced this difference to approximately 19%. The activating function A_x was found to be similarly affected with observed changes of comparable magnitude (Fig. 2(e)).

Similar results in shape and magnitude were also observed for a fiber parallel to the y-axis at a distance of 3 mm from the central axis of the stimulating electrode in the case of the electric potential (Fig. 2(b)), electric field (Fig. 2(d)) and activating function (Fig. 2(f)). The maximum percentage differences in the magnitude of the electric potential ϕ, the electric field E_x, and the activating function A_x, along a fiber of length 10 mm parallel to the x-axis at increasing perpendicular distance from the electrode are presented in Fig. 3.

When bipolar stimulation was applied, the difference in the electric potential, electric field and activating function between Models II–IV and Model I was less than 1% at a radial distance of 3 mm from the cathodic electrode contact.

3.3. Electrode located close to the skull

The electric potential, electric field and activating function resulting from an electrode located 3.5 mm from the boundary of the bulk tissue and cerebrospinal fluid layer were then compared in each of the models. Fig. 4 presents the electric potential, electric field and activating function for Models I–IV plotted along two arbitrary fiber axons. One fiber is parallel to the x-axis at a distance

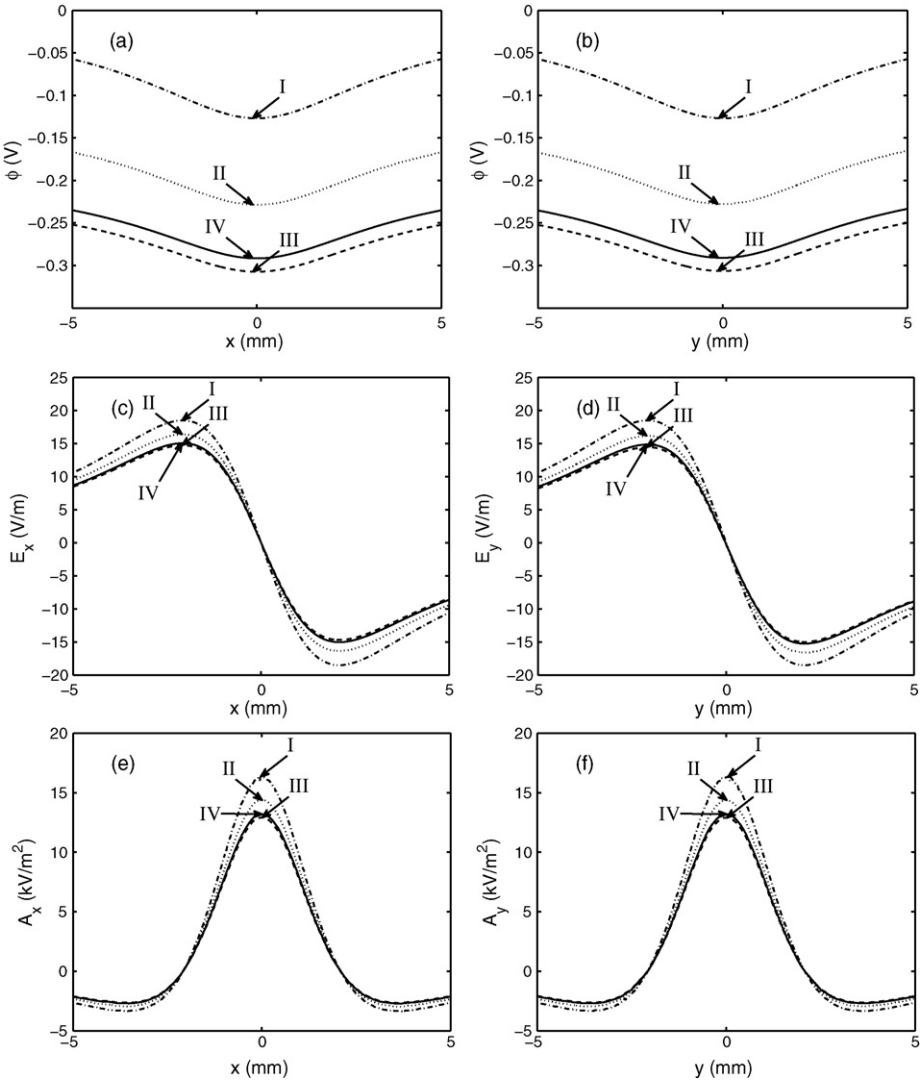

Fig. 2. Electric potential (a and b), electric field (c and d) and activating function (e and f) for an arbitrary fiber parallel to the x-axis at distance $y = 3$ mm from the central axis of the stimulating electrode, which is situated in the subthalamic nucleus. The electrode is parallel to the z-axis.

$y = -3$ mm from the central axis of the stimulating electrode. The other is parallel to the y-axis 3 mm away from the central axis of the stimulating electrode. The (x, y, z) co-ordinate system in the example presented is obtained by rotating the reference co-ordinate system (x', y', z') by $\alpha = 62^\circ$ about the z'-axis and by $\beta = 76^\circ$ about the x'-axis.

The effect of the finite volume and surrounding layers is presented in Fig. 4. The electric field (Fig. 4(d)) and activating function (Fig. 4(f)) were found to differ by a greater amount when the electrode was located close to the skull than when located close to the subthalamic nucleus. Additional localized contour effects were also observed in the surrounding region due to

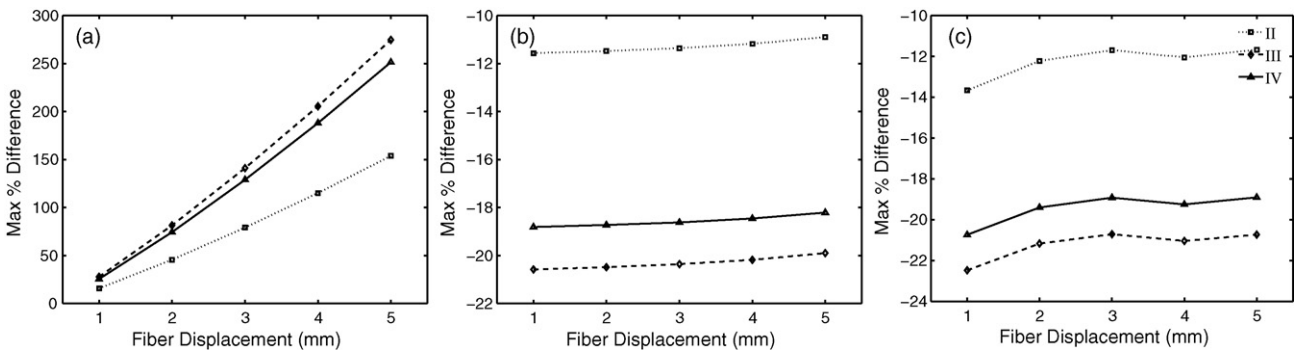

Fig. 3. Maximum percentage differences in the magnitude of the (a) electric potential ϕ, (b) the electric field E_x, and (c) the activating function A_x, along a fiber of length 10 mm parallel to the x-axis at distances of 1–5 mm from the central axis of the stimulating electrode (0.265–4.265 mm from the contact surface). Data is presented for models II (dotted), III (dashed), and IV (solid) relative to model I.

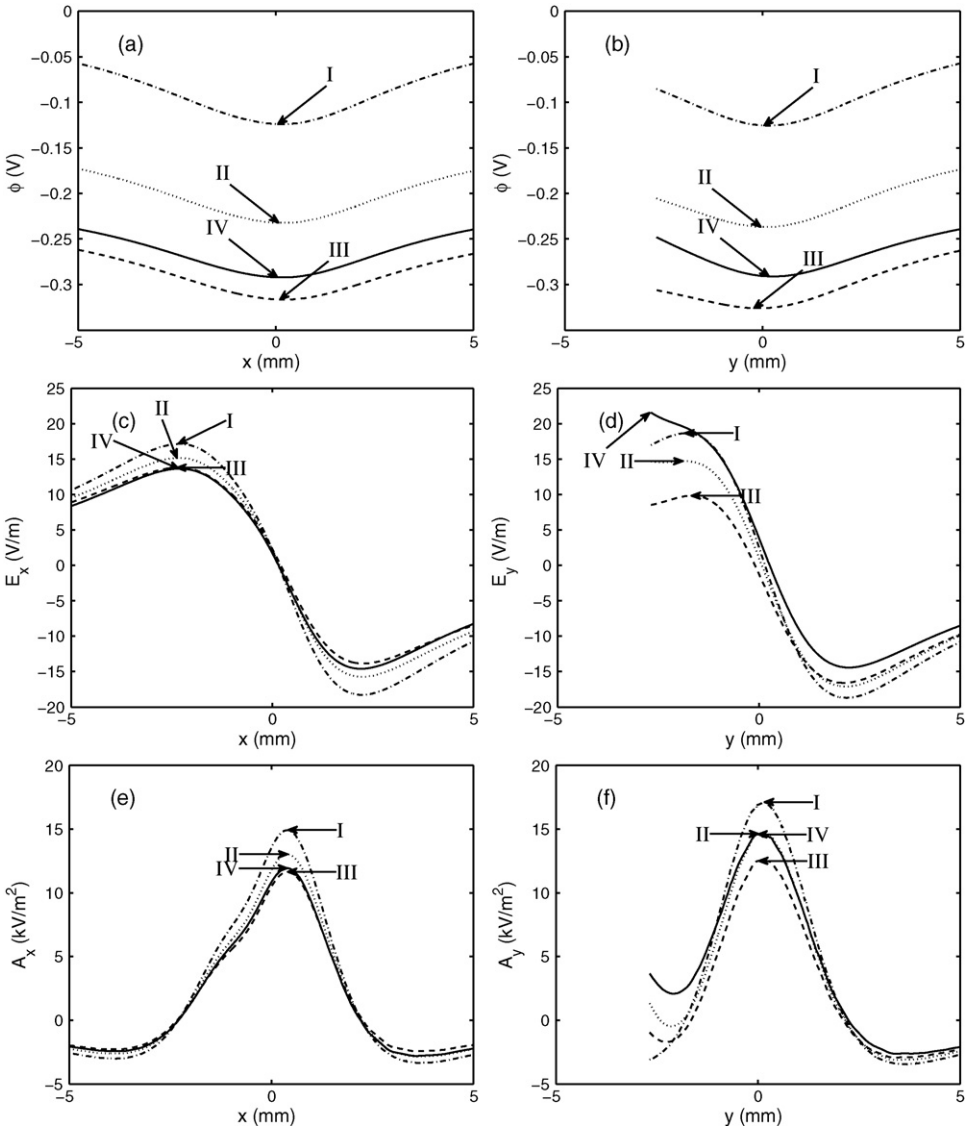

Fig. 4. Electric potential (a and b), electric field (c and d) and activating function (e and f) for an arbitrary fiber parallel to the x-axis at distance $y = 3$ mm from the central axis of the stimulating electrode, which is situated 3.5 mm from the cerebrospinal fluid. The plane in which the fibers lie is tilted with azimuth 62° and elevation 76° relative to a plane normal to the electrode's central axis. The fiber is truncated where it crosses the brain–CSF boundary (b, d and f).

the abrupt conductivity changes approaching the layer boundary (Fig. 5).

3.4. Sensitivity to tissue conductivity

The sensitivity of the effect of the finite volume and low-conductivity layers to changes in the conductivity of the skull bone, white matter and the encapsulation tissue was then analyzed, for the electrode located at position S_1, at the approximate location of the subthalamic nucleus. The maximum change in the potential, electric field, and activating function due to the incorporation of the finite volume and low conductivity layers is shown in Fig. 6. The effect of the finite volume and outer layers was observed to persist as the conductivity of the skull bone, bulk tissue and encapsulation tissue was altered.

4. Discussion

Previous finite element models of DBS have focused on the region of tissue immediately surrounding the electrode, neglecting

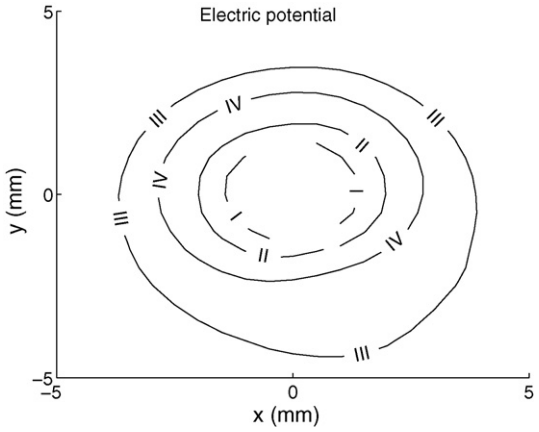

Fig. 5. Electric potential contour plot showing the 0.3 V contour level of Models I–IV across a 10 mm × 10 mm slice centered on the electrode at position S_2.

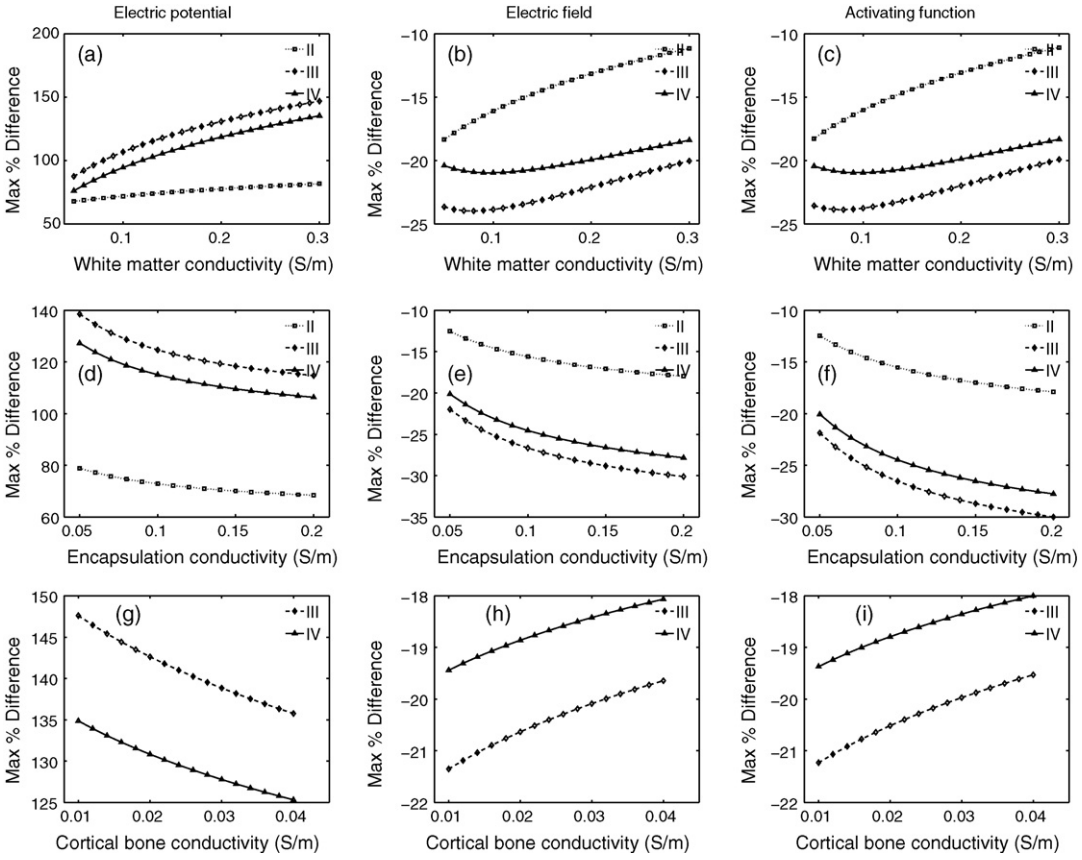

Fig. 6. Variation in the maximum percentage difference of the electric potential, electric field and activating function as the conductivity of the bulk tissue (a, b and c) and the electrode encapsulation tissue (d, e and f) was varied (Models II, III and IV) and as the conductivity of skull bone was varied (Models III and IV). Cancellous bone conductivity was scaled proportionally to that of cortical bone. Percentage differences are relative to Model I. Fiber positions as in Fig. 4.

the finite conducting volume of the head and the outer layers of scalp, skull and cerebrospinal fluid. By setting all outer boundaries to a potential of 0 V, such models approximate a situation of an isotropic ground located electrically far from the stimulating electrode. The purpose of this study was to examine whether the finite conducting volume, outer tissue layers and return electrode configuration could affect the electric field due to monopolar deep brain stimulation. In this case, the use of homogeneous isotropic brain tissue allows the effects of the finite conducting volume, outer tissue layers and return electrode configuration to be examined without compounding subject-specific effects.

The choice of electrical grounding was found to have a significant influence on the impedance observed between the stimulating electrode and the return electrode. The impedance in models which did not account for the finite conducting volume of the head, represented by Model I, was towards the lower end of the clinical range of 500–1500 Ω [3]. The reduced impedance is due to the constraint of current at the boundaries in Models II, III and IV, as shown in Table 2.

The impedance results also provide a measure of validation, since the impedance is an *in vivo* measurable quantity that can be checked during stimulator parameter settings. In previous models the impedance measurement has either been neglected, or has a form of compensation included to approximate clinically represented values. One method is to artificially increase the encapsulation layer thickness or impedance surrounding the electrode [13]. Alternatively the proportion of the surface area grounded can be reduced so as to satisfy the impedance requirement [34]. The results suggest that by incorporating a geometry that is anatomically based, impedance values can be obtained that closely approximate clinical data without artificial adjustment of the model.

The inclusion of a finite conducting volume was found to increase the magnitude of the electric potential by approximately 150–250% of its original value in the homogeneous cubic block where all outer surfaces were set to 0 V. The magnitude of the electric field and the activating function were consequently reduced by approximately 20% at locations close to the electrode (Fig. 2(a) and (b)). The change in potential observed is due to the more constrained path of the return current flow compared to homogeneous models. The presence of the low-conductivity skull and scalp layers in Models III–IV increased the electric potential and reduced the magnitude of the electric field and activating function. Due to high conductivity relative to the bulk tissue of the brain, the addition of the cerebrospinal fluid reduces the effect of the finite conducting volume. Although slightly counteracting the increase in potential, the magnitude of the change observed is relatively small and does not negate the effect of including the other layers and the overall finite conducting volume. The effect of the finite conducting volume and outer low-conductivity layers was preserved as the conductivity of the skull bone, the bulk tissue and the encapsulation tissue was systematically varied (Fig. 6). Bipolar stimulation was also examined, and the effect of the finite conducting volume and outer layers was found to be negligible. Therefore, the geometry and boundary conditions of Model I may be sufficient to capture the distribution of the activating function under bipolar stimulation.

When the electrode was located close to the skull, the contours of the electric potential, electric field and activating function

became distorted (Fig. 4(f)). The asymmetry observed in the shape of the electric potential, electric field and activating function was also affected by the direction of the fiber with respect to the electrode (Fig. 4(e)).

The effect of the finite conducting volume may become functionally significant when predicting the response of nearby neurons to monopolar DBS. The 20% difference in the peak magnitude of the activating function described in Figs. 2 and 4 may be sufficient to alter the number of simulated neurons that are activated. For example, it is possible that particular areas of the brain would not be activated as a result of DBS in Models II, III and IV, but would be in Model I. Given the small dimensions of the structures of interest, the inclusion or exclusion of the skull, scalp and cerebrospinal fluid layers may lead to different structures being activated or inhibited in the model. Such effects may become even more important if the bulk tissue volume is reduced for example when DBS is applied in children or adolescents [35]. The effect of the outer layers may also become significant when stimulation is close to the skull such as in models of cortical stimulation or other parts of the nervous system such as retinal prostheses and cochlear implants [36–39]. Increasing the accuracy of the predicted activating function could give better insight into the mechanisms of action and help to improve clinical outcomes by increasing the accuracy of estimates of regions of neural activation. Alternatively, a close approximation may be obtained by altering the tissue impedances to scale the resulting electric field. The use of computational modeling in emerging applications of deep brain stimulation may also benefit from a anatomically derived models such as that presented in this study [4–7].

A number of limitations of the model should be considered. Material properties for tissue conductivity vary considerably throughout the literature [31,40]. The use of the median frequency is a compromise that aims to represent the frequency-dependent material properties by those at a single frequency. Encapsulation tissue dimensions and material properties also vary among different studies [13], and there is wide variability in reported conductivity data for different biological tissues. Furthermore, many biological tissues, including brain tissue, are anisotropic [29]. Additionally, this model does not consider local tissue variations, nor does it include alternative return current paths caused by areas in the brain filled by cerebrospinal fluid. It is envisaged that detailed localized tissue maps could be combined with the macroscopic geometry presented here in practice [8,41]. Although the model has predicted localized contour effects when the electrode is located in close proximity to the outer layers, it is likely that further localized effects would be observed if subject-specific variations were incorporated. The model has considered a DC steady-state analysis and does not incorporate capacitive or dispersive effects. Therefore the frequency-dependent bulk tissue properties are not considered. The electrode–tissue interface has been neglected and the electrical double-layer formed at the interface is not included [42]. The activating function itself allows approximate estimates of areas of activation to be made, but does not take into account other factors affecting activation such as axon diameter [43]. Alternative formations can allow curved fibers to be examined [44]. Nevertheless, based on the results presented in this study, it has been shown that the incorporation of the finite volume of the head with localized surface reference electrode and cerebrospinal fluid, skull and scalp layers does alter the distribution of the electric field due to deep brain stimulation.

Acknowledgment

This work was funded by Science Foundation Ireland Grant 05/RF/ENM047.

Conflict of interest statement

The authors of this manuscript have no conflicts of interest.

References

[1] McIntyre CC, Savasta M, Walter BL, Vitek JL. How does deep brain stimulation work? Present understanding and future questions. J Clin Neurophysiol 2004;21(1):40–50.
[2] McIntyre CC, Savasta M, Kerkerian-Le Goff L, Vitek JL. Uncovering the mechanism(s) of action of deep brain stimulation: activation, inhibition, or both. Clin Neurophysiol 2004;115(6):1239–48.
[3] Volkmann J, Herzog J, Kopper F, Deuschl G. Introduction to the programming of deep brain stimulators. Mov Disord 2002;17(Suppl. 3):S181–7.
[4] Berlin HA, Hamilton H, Hollander E. Experimental therapeutics for refractory obsessive-compulsive disorder: translational approaches and new somatic developments. Mt Sinai J Med 2008;75(May–June (3)):174–203.
[5] Houeto JL, Karachi C, Mallet L, Pillon B, Yelnik J, Mesnage V, et al. Tourette's syndrome and deep brain stimulation. J Neurol Neurosurg Psychiatry 2005;76(July (7)):992–5.
[6] Mayberg HS, Lozano AM, Voon V, McNeely HE, Seminowicz D, Hamani C, et al. Deep brain stimulation for treatment-resistant depression. Neuron 2005;45(March (5)):651–60.
[7] Theodore WH, Fisher RS. Brain stimulation for epilepsy. Lancet Neurol 2004;3(February (2)):111–8.
[8] Sotiropoulos SN, Steinmetz PN. Assessing the direct effects of deep brain stimulation using embedded axon models. J Neural Eng 2007;4(2):107–19.
[9] Yousif N, Bayford R, Wang S, Liu X. Quantifying the effects of the electrode–brain interface on the crossing electric currents in deep brain recording and stimulation. Neuroscience 2008;152(March (3)):683–91.
[10] Wei XF, Grill WM. Current density distributions, field distributions and impedance analysis of segmented deep brain stimulation electrodes. J Neural Eng 2005;2(4):139–47.
[11] Astrom M, Johansson JD, Hariz MI, Eriksson O, Wardell K. The effect of cystic cavities on deep brain stimulation in the basal ganglia: a simulation-based study. J Neural Eng 2006;3(2):132–8.
[12] Yousif N, Bayford R, Bain PG, Liu X. The peri-electrode space is a significant element of the electrode–brain interface in deep brain stimulation: a computational study. Brain Res Bull 2007;74(5):361–8.
[13] Butson CR, Maks CB, McIntyre CC. Sources and effects of electrode impedance during deep brain stimulation. Clin Neurophysiol 2006;117(2):447–54.
[14] McIntyre CC, Grill WM, Sherman DL, Thakor NV. Cellular effects of deep brain stimulation: model-based analysis of activation and inhibition. J Neurophysiol 2004;91(4):1457–69.
[15] Stok CJ. The influence of model parameters on EEG/MEG single dipole source estimation. IEEE Trans Biomed Eng 1987;34(4):289–96.
[16] Eshel Y, Witman S, Rosenfeld M, Abboud S. Correlation between skull thickness asymmetry and scalp potential estimated by a numerical model of the head. IEEE Trans Biomed Eng 1995;42(3):242–9.
[17] Gootzen TH, Stegeman DF, Van Oosterom A. Finite limb dimensions and finite muscle length in a model for the generation of electromyographic signals. Electroencephalogr Clin Neurophysiol 1991;81(2):152–62.
[18] Wagner TA, Zahn M, Grodzinsky AJ, Pascual-Leone A. Three-dimensional head model simulation of transcranial magnetic stimulation. IEEE Trans Biomed Eng 2004;51(9):1586–98.
[19] Pollack P, Benabid AL, Krack P, Limousin P, Benazzouz A. Deep brain stimulation. In: Parkinson's disease and movement disorders. Williams and Wilkins; 1998. p. 1085–101.
[20] Kuncel AM, Grill WM. Selection of stimulus parameters for deep brain stimulation. Clin Neurophysiol 2004;115(11):2431–41.
[21] Rattay F. Modeling the excitation of fibers under surface electrodes. IEEE Trans Biomed Eng 1988;35(3):199–202.
[22] Bouchet LG, Bolch WE, Weber DA, Atkins HL, Poston Sr JW. A revised dosimetric model of the adult head and brain. J Nucl Med 1996;37(7):1226–36.
[23] Oozeer M, Veraart C, Legat V, Delbeke J. Simulation of intra-orbital optic nerve electrical stimulation. Med Biol Eng Comput 2005;43(September (5)):608–17.
[24] International Commission of Radiological Protection. Report of the task group on reference man. Oxford Pergamon Press; 1975.
[25] Scheufler O, Kania NM, Heinrichs CM, Exner K. Hyperplasia of the subcutaneous adipose tissue is the primary histopathologic abnormality in lipedematous scalp. Am J Dermatopathol 2003;25(3):248–52.
[26] Medtronic, Inc. 3387–3389 lead kit for deep brain stimulation - implant manual. Minneapolis, MA; 2006.
[27] Agur AMR, Lee JM, Grant JCB. Grant's atlas of anatomy. Lippincott, Williams and Wilkins; 1999.
[28] Grill WM, Mortimer JT. Electrical properties of implant encapsulation tissue. Ann Biomed Eng 1994;22(September (1)):23–33.
[29] Ranck JB, BeMent Jr SL. The specific impedance of the dorsal columns of the cat: an inisotropic medium. Exp Neurol 1965;11:451–63.
[30] Baumann SB, Wozny DR, Kelly SK, Meno FM. The electrical conductivity of human cerebrospinal fluid at body temperature. IEEE Trans Biomed Eng 1997;44(3):220–3.

[31] Gabriel S, Lau RW, Gabriel C. The dielectric properties of biological tissues. III. Parametric models for the dielectric spectrum of tissues. Phys Med Biol 1996;41(11):2271–93.
[32] Plonsey R, Heppner DB. Considerations of quasi-stationarity in electrophysiological systems. Bull Math Biophys 1967;29(4):657–64.
[33] Holsheimer J, Dijkstra EA, Demeulemeester H, Nuttin B. Chronaxie calculated from current-duration and voltage-duration data. J Neurosci Methods 2000;97(1):45–50.
[34] Hemm S, Mennessier G, Vayssiere N, Cif L, El Fertit H, Coubes P. Deep brain stimulation in movement disorders: stereotactic coregistration of two-dimensional electrical field modeling and magnetic resonance imaging. J Neurosurg 2005;103(6):949–55.
[35] Alterman RL, Tagliati M. Deep brain stimulation for torsion dystonia in children. Childs Nerv Syst 2007;23(9):1033–40.
[36] Alonso-Alonso M, Fregni F, Pascual-Leone A. Brain stimulation in poststroke rehabilitation. Cerebrovasc Dis 2007;24(Suppl. 1):157–66.
[37] Manola L, Holsheimer J, Veltink P, Buitenweg JR. Anodal vs cathodal stimulation of motor cortex: a modeling study. Clin Neurophysiol 2007;118(2):464–74.
[38] Rattay F, Resatz S. Effective electrode configuration for selective stimulation with inner eye prostheses. IEEE Trans Biomed Eng 2004;51(9):1659–64.
[39] Lim YS, Park S-I, Kim YH, Oh SH, Kim SJ. Three-dimensional analysis of electrode behavior in a human cochlear model. Med Eng Phys 2005;27(October (8)):695–703.
[40] Geddes LA, Baker LE. The specific resistance of biological material—a compendium of data for the biomedical engineer and physiologist. Med Biol Eng 1967;5(3):271–93.
[41] Butson CR, Cooper SE, Henderson JM, McIntyre CC. Patient-specific analysis of the volume of tissue activated during deep brain stimulation. Neuroimage 2007;34(2):661–70.
[42] Cantrell DR, Inayat S, Taflove A, Ruoff RS, Troy JB. Incorporation of the electrode–electrolyte interface into finite-element models of metal microelectrodes. J Neural Eng 2008;5(1):54–67.
[43] Rattay F. Analysis of models for external stimulation of axons. IEEE Trans Biomed Eng 1986;33(10):974–7.
[44] Iles JF. Simple models of stimulation of neurones in the brain by electric. Prog Biophys Mol Biol 2005;87(January (1)):17–31.